

## EXPANDING THE CHARA/FLUOR HOT DISKS SURVEY

B. MENNESSON<sup>\*,††</sup>, N. SCOTT<sup>†</sup>, T. TEN BRUMMELAAR<sup>†</sup>, G. BRYDEN<sup>\*</sup>, N. TURNER<sup>\*</sup>,  
O. ABSIL<sup>‡</sup>, R. MILLAN-GABET<sup>§</sup>, V. COUDE DU FORESTO<sup>¶</sup>, J. C. AUGEREAU<sup>||</sup>,  
S. RIDGWAY<sup>\*\*</sup>, J. LEBRETON<sup>||</sup> and L. MARION<sup>‡</sup>

<sup>\*</sup>Jet Propulsion Laboratory, California Institute of Technology  
4800 Oak Grove Drive, Pasadena CA 91109-8099, USA

<sup>†</sup>Center for High Angular Resolution Astronomy  
Georgia State University  
Mt. Wilson, CA 91023, USA

<sup>‡</sup>Departement d'Astrophysique, Geophysique et Oceanographie  
Université de Liege, 17 Allée du Six Aout  
B-4000 Sart Tilman, Belgium

<sup>§</sup>NASA Exoplanet Science Center (NExSci), California Institute of Technology  
770 South Wilson Avenue, Pasadena CA 91125, USA

<sup>¶</sup>Observatoire de Paris, Section de Meudon  
F-92195 Meudon Principal Cedex, France

<sup>||</sup>IPAG, UMR 5274, CNRS and Université Joseph Fourier  
BP 53, F-38041 Grenoble, France

<sup>\*\*</sup>National Optical Astronomy Observatory, P. O. Box 26732  
Tucson, AZ 85726-6732, USA

<sup>††</sup>Bertrand.Mennesson@jpl.nasa.gov

*Received 2013 July 22; Revised 2013 November 5; Accepted 2013 November 6; Published 2014 January 6*

Little is presently known about the hot (>300 K) dust component of debris disks surrounding main sequence stars, similar to the zodiacal dust cloud found in the inner solar system. While extensive surveys have been carried out from space, the majority of detections have surprisingly come from the ground, where near infrared interferometric observations have recently revealed small (~1%) resolved excesses around a dozen nearby main sequence stars. Most of these results have come from the CHARA array “FLUOR” instrument (Mt. Wilson, CA), which has demonstrated the best sensitivity worldwide so far for this type of studies, and has carried out an initial survey of ~40 stars. In order to further understand the origin of this “hot dust phenomenon”, we will extend this initial survey to a larger number of stars and lower excess detection limits, i.e. higher visibility accuracy providing higher contrast measurements. To this end, two major instrumental developments are underway at CHARA. The first one aims at improving FLUOR’s sensitivity to a median K-band magnitude limit of 5 (making 200 targets available). The second development is based on a method that we recently developed for accurate (better than 0.1%) null depth measurements of stars, and that can be extended to regular interferometric visibility measurements.

*Keywords:* Instrumentation: interferometers, zodiacal dust.

### 1. Introduction

One of the most intriguing results of high angular resolution observational astrophysics in the last few years is the detection of hot (1000–1500 K) dust populations (bright “exozodiacal disks” or dust belts) around a significant fraction (25–30%) of

nearby main sequence stars (Absil *et al.*, 2013). These dust grains, located within the first AU from their parent stars, are thought to be produced by collisions between larger rocky bodies and/or by the evaporation of comets, as in the solar zodiacal disk. The detected disks are however much

hotter and more massive than the zodiacal cloud, and presumably formed of much smaller grains (sub-micron sized). Such grain populations should be expelled from the inner planetary system by radiation pressure within only a few years, which could indicate inordinate replenishment rates or unknown dust trapping mechanisms. In practice, the steady state collisional grinding of a massive asteroid belt cannot be at the origin of these hot populations (Wyatt *et al.*, 2007). They are rather most likely produced by isolated catastrophic events (e.g. major asteroid collision, break-up of a massive comet), or by major dynamical perturbations such as the Falling Evaporating Bodies (FEB) phenomenon in the  $\beta$  Pictoris inner disk (Beust & Morbidelli, 2000; Thebault & Beust, 2001) or the Late Heavy Bombardment (LHB, Gomes *et al.*, 2005) that happened early in the history of our own planetary system. LHB-like events have already been invoked to explain the existence of bright warm ( $\sim 300$  K) debris disks around mature stars, such as HD 69830 (Beichman *et al.*, 2005) and  $\eta$  Corvi (Smith *et al.*, 2009). Processes at play in the hotter debris disks may be similar, as recent dynamical modeling suggests that during the LHB, outer planets scattered numerous comets in the inner solar system, causing substantial ( $>10^4$ ) and durable brightening (10–100 Myr) of the inner zodiacal cloud infrared luminosity (Nesvorný *et al.*, 2010). Most of these hot debris disk discoveries have only been recently made possible thanks to high-accuracy infrared interferometric measurements at Keck (Millan-Gabet *et al.*, 2011), VLT (Absil *et al.*, 2009), the MMT (Stock *et al.*, 2010), IOTA (Defrere *et al.*, 2011) and especially at Mount Wilson’s CHARA array (McAlister *et al.*, 2000; Absil *et al.*, 2006, 2008, 2009 & 2013; Di Folco *et al.*, 2007; Akeson *et al.*, 2009). The latter CHARA detections used the “FLUOR” (Fiber Linked Unit for Optical Recombination) near infrared (NIR) instrument installed in 2004, and have been the most numerous so far. Overall, the detection of hot dust populations, producing NIR excesses at the  $\sim 1\%$  level and residing in the first few AU, has now been established around 12 nearby single main sequence AFGK stars (Absil *et al.*, 2009, 2013) out of about 40 sampled so far. In comparison, 10 of these stars have also been observed at the Keck Observatory (Millan-Gabet *et al.*, 2011; Mennesson *et al.*, in prep) using mid-infrared (MIR) nulling interferometry, a technique that provides a dynamic

range similar to that of CHARA/FLUOR. Surprisingly, only 2 of these stars ( $\beta$  Leo: Stock *et al.*, 2010, and Fomalhaut: Mennesson *et al.*, 2013) showed a detectable MIR (8 to 13 microns) excess. In the particular case of Fomalhaut, a detailed radiative transfer modeling of the exozodiacal disk was performed (Lebreton *et al.*, 2013). A good fit to the data was found with two distinct dust populations: (i) very small, hence unbound, hot dust grains confined in a narrow region at the sublimation rim of carbonaceous material; (ii) bound grains at 2 AU that are protected from sublimation and have a higher mass despite their fainter flux level. It is further suggested that the hot dust is produced by the release of small carbon grains following the disruption of aggregates that originate from the warm component. If confirmed around more stars, this scenario would imply that the hot dust component responsible for the NIR excess may just be “the tip of the iceberg”, since it may originate from a (comparatively harder to detect) counterpart residing further out, near the ice line. For all of these reasons, we have decided to extend the current NIR hot disk survey carried out with CHARA/FLUOR to a larger number of stars and to higher contrast.

## 2. NIR Hot Disk Survey Instrumental Specifications

The default view of exozodi observational studies is that MIR surveys should be more sensitive to warm dust than NIR surveys. Indeed, if exozodiacal clouds were analogous to the solar system case in terms of spatial and spectral brightness distributions, the overall dust flux relative to the star would be about 60 times higher at 10 microns than at 2 microns (Kelsall *et al.*, 1998). Consequently, most of the exozodi characterization efforts have been concentrating so far on the MIR domain, as illustrated by the nulling surveys conducted from the Keck Telescopes and just starting at the Large Binocular Telescope Interferometer (LBTI). A natural requirement for our NIR survey is then to improve on the performance of MIR surveys. More precisely, our instrumental specifications are derived from three main requirements: (i) access sufficient spatial resolution, (ii) reach fainter limiting magnitude than past or current MIR facilities, and (iii) achieve equivalent or deeper contrast levels than past MIR surveys. Additionally, and as noted in the previous section, some observational and modeling results suggest that exozodi clouds exhibit

very non-solar characteristics, and that even at the same contrast performance, they may actually be more easily and abundantly detected in the NIR than in the MIR.

### 2.1. Spatial resolution: Why infrared interferometry?

Exozodiacal disks are optically thin and represent very little mass compared to their host stars. As a result, they produce no gravitational effect detectable by traditional indirect detection techniques such as radial velocity or astrometry. Accurate transit observations of favorably inclined systems may be useful if strong disk asymmetries are present (Stark, 2011). But in the general case, debris disks around nearby stars will be better detected through their extra emission. While cold debris disks cause very significant excesses readily detectable at mid to far infrared wavelengths, exozodiacal material located in the inner few AU only contributes a small fraction of the stellar flux. In order to reliably detect such tiny ( $< \sim 1\%$ ) excess emission over that expected from the photosphere, direct detection is required, with the ability to spatially resolve dust from the central star. With the spatial scales at play, typically 0.1 to a few AU, and targeting a sample of main sequence stars within  $\sim 50$  pc, this corresponds to angular separations of a milliarcsec or so. In the infrared, such resolution can only be achieved using long baseline interferometry. The CHARA array offers baselines ranging from 34 m to 300 m, which provides largely enough resolution for this type of studies. In fact CHARA's shortest baselines of 34 m and 66 m are optimum, as they can resolve dust without resolving the stellar photospheres significantly, i.e. the uncertainty on the stellar diameter is generally not an issue at these baselines (Absil *et al.*, 2013). Finally, even if exozodiacal disks are expected to show clumpy structures and some degree of asymmetry, this remains a second degree effect and possible phase closure signatures will be even smaller than visibility effects. Accurate NIR visibility *amplitude* measurements appear then as the technique of choice for the ground-based detection of faint exozodiacal disks.

### 2.2. Sensitivity

Space telescopes can reach a fairly high sensitivity in the MIR, but they do not spatially resolve dust emission and rely on model fitting to detect any departure from pure photospheric emission. As a

result, they are limited to a dynamic range of  $\sim 30:1$  around 10 microns (e.g. Spitzer IRS survey of debris disks around  $\sim 200$  solar type stars, Lawler *et al.*, 2009) and cannot detect excesses lower than a few percent.

Conversely, ground-based MIR interferometric observations allow to spatially resolve the dust and reach deeper contrast levels, but their sensitivity is strongly reduced by the large thermal background arising from sky and optics emission. In practice, ground-based MIR exozodi surveys are limited to stars brighter than about 1 Jy at 10 microns. This is illustrated by 8–10-m class telescope observations carried recently with the Keck Telescopes (Millan-Gabet *et al.*, 2011) and those just starting at the Large Binocular Telescope (Roberge *et al.*, in prep). Depending on the stellar spectral type (A to K), this 1 Jy flux limit at 10 microns corresponds to a typical NIR limiting magnitude (e.g. K-band) of about 3 to 4, which can be achieved with interferometric arrays of  $\sim 1$ -m telescopes. In fact, the past CHARA/FLUOR hot disk survey already reached a limiting K magnitude of  $\sim 4$  (Absil *et al.*, 2013). It was enough to observe 40 nearby main sequence single stars, half of them with a known far infrared excess (“cold dust sub-sample”) detected by IRAS, Spitzer/MIPS or Herschel/PACS observations, and the other half with no previous evidence of circumstellar excess (“non dusty” sub-sample). As shown in Fig. 1, improving the CHARA/FLUOR limiting K magnitude to 5 would already allow to extend the survey to slightly over 200 stars, still keeping a  $\sim 50/50$  split between dusty and *a priori* non-dusty stars and a fairly uniform repartition of spectral types. Going from 40 to  $\sim 200$  stars would improve the statistical significance of currently inferred trends of NIR excess versus basic stellar parameters such as age, spectral type, the known presence of cold dust or planets in the system. As a result, we have set a requirement of  $K = 5$  for the extended CHARA/FLUOR hot disk survey “median” limiting magnitude, i.e. obtained under typical seeing conditions.

A number of sensitivity upgrades have recently taken place or are on the way with CHARA/FLUOR. The FLUOR beam (pupil) has been carefully co-aligned to the main CHARA boresight beam, hence eliminating any source of differential vignetting between the CHARA telescopes and the FLUOR instrument. The scanning mirrors used for optimization of the starlight

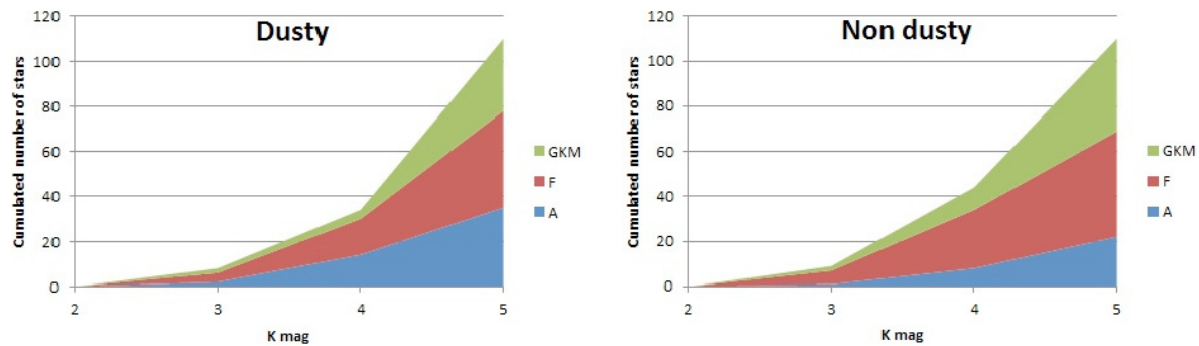


Fig. 1. Cumulated number of sample stars brighter than a given K magnitude. Left: stars with a mid/far infrared excess detected by SPITZER (MIPS 24 or 70 micron) or Herschel/PACS. Right: “control sample” of stars with no such excess detected. There are 110 stars per category, i.e. 220 in total. During any given run, observations follow this dusty/non-dusty star pairing rule. Note the important gain of improving the CHARA/FLUOR sensitivity from  $m_K = 3-4$  to  $m_K = 5$ . All stars in the overall sample are presumably single stars, in order to avoid contamination of the observed visibility by a companion located within the interferometric field of view ( $\sim 1''$ ).

coupling into FLUOR single-mode fibers have been replaced, providing much higher pointing accuracy and repeatability onto the fiber tips. During our last CHARA/FLUOR observing run (October 10–19, 2013), these improvements have already allowed to record fringes on a few stars with  $K = 5$  under very average seeing conditions (estimated  $r_0$  of  $\sim 5$  cm in the visible). Some further gain is expected thanks to the on-going development of a CHARA telescopes adaptive optics (AO) system (Ridgway *et al.*, 2008). It has seen its first phase approved by the NSF (April 2011), aiming at improved tip-tilt correction and tip-tilt measurement sensitivity (correction at the telescope level rather than close to recombination), plus some static correction of wavefront errors after propagation to the lab. All parts and dichroics have been procured, and the new tip-tilt system is currently being tested on the first of the 6 CHARA telescopes. These tip-tilt improvements will provide higher injection efficiency into FLUOR’s single-mode fibers, yielding sensitivity to fainter stars and better photometric stability at a given magnitude. Finally, we have plans to improve the instrument point source visibility, which promises some further gain in fringe detection sensitivity. As a summary, we are confident that high quality visibility measurements will be routinely achieved with FLUOR down to  $K = 5$  or even 6 in 2014.

### 2.3. Contrast requirement and current performance

While operating in the NIR provides an obvious sensitivity advantage over MIR ground-based

observations, the effects of atmospheric turbulence and optical aberrations are larger at shorter wavelengths, making high accuracy visibility measurements *a priori* more challenging in the NIR than in the MIR. The best contrast achieved so far by MIR interferometric observations corresponds to a null depth measurement uncertainty of 0.2%, as demonstrated on bright sources ( $>5$  Jy) by the Keck Interferometer (KI) Nuller (Colavita *et al.*, 2009). Remarkably, the median uncertainty of the excess measurements carried out so far by CHARA/FLUOR is also 0.2% (Absil *et al.*, 2013), which translates into a relative visibility accuracy of 0.4%. It is worth noting that this number refers to the *final* visibility accuracy based on 5 to 10 measurements per star. The individual visibility measurement uncertainty is closer to 1% (Merand *et al.*, 2006). As explained above, this current performance was already sufficient to detect more excesses in the NIR than in the MIR, and can hence be regarded as a minimum requirement for the extended CHARA/FLUOR hot disk survey. However, we would like to improve on this value and our goal is to reach an individual visibility accuracy of 0.2%, about 5 times better than the current performance. While this value is somewhat arbitrary, such substantial improvement would allow to keep up with the MIR domain, where a  $\sim$ tenfold contrast improvement is expected in the near future thanks to the LBTI exozodi survey. This 0.2% CHARA/FLUOR visibility accuracy requirement is also consistent with separate preliminary results that we obtained at other NIR interferometers (see Sec. 3).

## 2.4. Current limitations and expected improvements

The accessible dynamic range of ground-based optical/infrared interferometers is limited by the measurement accuracy of phase closure or visibility amplitudes, which are plagued by systematic effects. In the present case of visibility amplitude measurements (disks brightness distributions are centrally symmetric to first order), the observation of a given star yields a measured value  $V_m = V \cdot T_i$ , where  $V$  is the actual object’s visibility — directly related to its brightness distribution, including the star plus any extended extra emission — and  $T_i$  ( $<1$ ) is the “instrumental” transfer function, i.e. the visibility that would be measured on a point source. In practice, this unknown instrumental visibility term is the largest source of noise and potential bias in the estimation of the true underlying object’s visibility. When operating in the MIR, one possible solution is to carefully design the instrument so that  $T_i$  is permanently kept to a stable value close to 1. This is the approach retained by the successive mid-infrared nulling interferometers built at the MMT, Keck and LBT observatories. Conversely, when observing in the NIR, atmospheric effects and corresponding phase corrugations are much larger than static instrumental effects: most of the time variability of the instrumental function comes from atmospheric turbulence, whose characteristics change rapidly, causing a larger and highly variable coherence loss both within an observation, and between successive stellar observations. An attractive solution is to measure this fluctuating atmospheric term using single-mode fibers for recombination (Coude du Foresto *et al.*, 1998; Mennesson *et al.*, 2002). In that case, the individual beam phase corrugations created by the rapidly changing atmosphere are traded against intensity fluctuations, which are monitored in real time. Only the global optical path difference (OPD) or “piston” between the beams remains. Using this technique, FLUOR achieved the most accurate visibility measurements recorded by NIR long baseline interferometry so far, with ( $1\sigma$ ) relative visibility accuracy better than 1% per calibrated observation (Perrin *et al.*, 1998; Merand *et al.*, 2006) of bright stars ( $m_K < 3$ ), and a residual floor of about 0.2% rms when averaging several sequences at the same baseline. Although quite impressive, FLUOR’s current accuracy is still limited by two well-identified factors: chromatic

biases, and “piston” (OPD jitter) noise, which we discuss hereafter.

The introduction of a dispersed FLUOR mode — now 8 spectral channels available inside K-band — will strongly reduce any residual chromatic bias. More precisely, broad-band measurements are affected by the FLUOR “shape factor” (Coude du Foresto *et al.*, 1997), which is a function of stellar spectrum within the observing bandwidth, and which generally differs between the target and its calibrator(s). This effect will be completely negligible in FLUOR dispersed mode or when using narrow band ( $<50$  nm bandwidth) filters. Similarly, differential atmospheric refraction effects due to observing target and calibrator(s) at slightly different zenith angles will be strongly reduced, and are expected to be negligible when using FLUOR dispersed mode. Incidentally, this mode will also explore the wavelength dependence of the excess and help constrain its origin: a relative excess increasing with wavelength could for instance indicate thermal emission rather than starlight scattering.

In order to detect fringes, the FLUOR instrument currently uses a fast temporal modulation of the Optical Path Difference (OPD) to scan through the broad-band fringe packet, and measures visibilities in the Fourier domain (Coude du Foresto *et al.*, 1997). In the presence of atmospheric piston, some of the fringes energy is being redistributed at different frequencies than the scan frequency and the overall energy (related to the object’s visibility) is not conserved. In general, these piston effects will be slightly different between the target and its calibrator(s), causing a small calibration error. While the extended FLUOR survey will start with this regular data acquisition (scan) and reduction approach (Coude du Foresto *et al.*, 1997), we will use a new data acquisition/reduction approach to improve the current visibility accuracy. This approach is inspired by a method we originally developed for deep NIR null measurements. But it can be generalized to “regular” visibility measurements, and equally applies to cases where the astronomical source is significantly resolved. The method’s overall principle, some relevant results and the envisioned CHARA/FLUOR implementation are discussed in details in the next section.

## 3. Visibility Self Calibration (VSC)

A key ingredient to the extended FLUOR hot disk survey is the adaptation of “Null Self Calibration”

(NSC), a statistical data analysis technique that we recently developed (Mennesson *et al.*, 2011a; Hanot *et al.*, 2011), and which we plan to apply to fringe tracked FLUOR data. In this approach, the interferometric signal is rapidly recorded (every few ms) close to a “fixed” (jitter  $< \sim \lambda/5$  rms) optical path difference (OPD) position corresponding to the fringe packet lowest point (i.e. the central broadband dark fringe).

### 3.1. VSC principle

The VSC principle is similar to the Null Self Calibration (NSC) approach. The only difference is that in the VSC case, we do not require that the object’s visibility be close to 1, nor that deep (instantaneous) null measurements be measured. For VSC (or NSC) to be effective, four main conditions are required: (i) the beams shall eventually be recombined in a common single-mode waveguide, (ii) the interferometric signal must be sampled significantly faster than the atmospheric coherence time (or fringe tracker closed loop bandwidth), (iii) the OPD must be stabilized around the central dark fringe of the fringe packet with no fringe hop ( $\sim \lambda/5$  rms jitter is small enough), (iv) background and individual beam signals must be recorded close in time to the fringe data.

In the single-mode recombination case, and assuming monochromatic radiation, the interferometric signal  $I(t)$  is only affected by intensity and phase mismatches between the beams. It reads as:

$$I(t) = I_1(t) + I_2(t) + 2|V| \cdot \sqrt{I_1(t) \cdot I_2(t)} \cdot \cos(\phi(t) + \phi_V) + B(t),$$

where  $I_{1,2}(t)$  are the instantaneous beam intensities,  $\phi(t)$  is their phase difference,  $|V| \cdot \exp(j \cdot \phi_V)$  is the target’s complex visibility and  $B(t)$  is the background signal (including detector bias plus any thermal emission). In the case where data are recorded around the central dark fringe, noting  $\Delta\phi(t)$  the instantaneous phase offset from  $\pi$ , the expression becomes:

$$I(t) = I_1(t) + I_2(t) - 2|V| \cdot \sqrt{I_1(t) \cdot I_2(t)} \cdot \cos(\Delta\phi(t)) + B(t).$$

The VSC (NSC) method is based on the analysis of the measured probability distribution of  $I(t)$ , which is noted  $p_I$ . If the signals  $I_{1,2}(t)$  and  $B(t)$  are measured close enough to  $I(t)$  or at the same time, their statistical distributions can be very well estimated

and their effect can essentially be “taken out” of  $p_I$ . As for the phase error term  $\Delta\phi(t)$ , its actual distribution can either be retrieved from fringe tracker data if available, or it can be assumed to be Gaussian with mean  $\mu$  and standard deviation  $\sigma$  (a very legitimate approximation for fringe tracked data obtained at KI). At this stage, there are only 3 free parameters left in the observed distribution  $p_I$ : the Gaussian phase error parameters  $(\mu, \sigma)$ , and the object’s visibility  $V$ . Using the measured signals  $I_{1,2}(t)$  and  $B(t)$ , a fake sequence of temporal signals  $I'(t, \mu, \sigma, V)$  is then generated for all possible values of the free parameters. The resulting probability distribution  $p_{I'}$  is computed for each triplet  $(\mu, \sigma, V)$  and compared to the observed distribution  $p_I$ . The parameters values are then adjusted to match the model and observed distributions minimizing a goodness of fit Pearson  $\chi^2$  test (Hanot *et al.*, 2011). The main output of this fitting procedure is the object’s visibility  $V$ , or equivalently its astronomical null defined as  $(1 - V)/(1 + V)$ .

The NSC method was first demonstrated with the NIR Palomar Fiber Nuller (PFN), achieving visibility accuracy measurements better than 0.1%, while early VSC testing at the Keck Interferometer indicates better than 0.2% rms visibility stability at K-band. Both experimental results are described hereafter before discussing plans for implementing the method at CHARA/FLUOR.

### 3.2. Null self calibration with the PFN

The Palomar fiber Nuller (PFN) is a “mini” NIR (broad K-band) nulling interferometer developed at JPL since 2006 (e.g. Mennesson *et al.*, 2006). It uses two ( $3 \times 1.5$  m) sub-aperture beams of the primary mirror located 3.2 m apart and recombines them into a common single-mode fiber, as in the case of CHARA/FLUOR. It is a visitor instrument installed in the Palomar 200 inch Cassegrain cage and located downstream of the AO system which stabilizes the 2 beams OPD down to  $\sim 200$  nm rms at K-band. Using the VSC approach described above in the particular case where the source is mostly unresolved ( $V \sim 1$  and astronomical null close to zero), the PFN routinely produces visibility measurements with accuracies better than 0.1%. Figure 2 shows as an illustration the results obtained on the bright star  $\alpha$  Boo, for which consecutive NSC estimates were derived over 1 hr of observation and remained stable at the few  $10^{-4}$  level. Note that for the PFN, we computed the observed

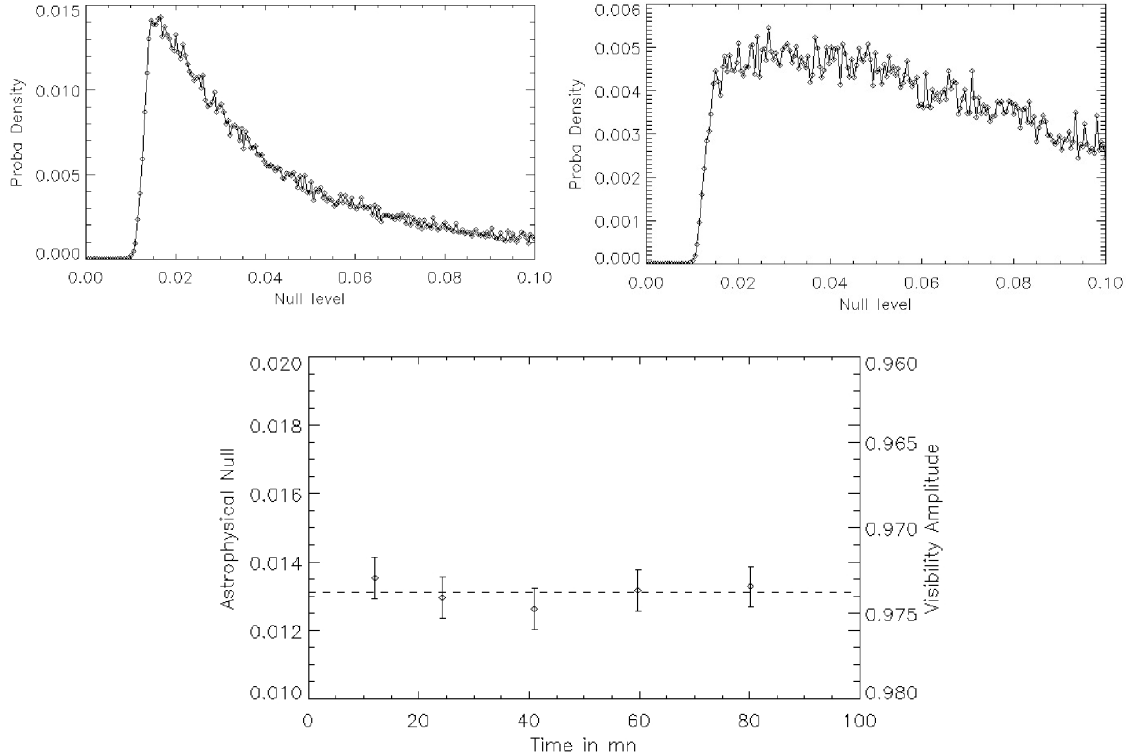


Fig. 2. Palomar Fiber Nuller measurements of  $\alpha$  Boo. Top panels: observed distributions of instantaneous interferometric signals (normalized to constructive interference case to provide an instantaneous “null” level) recorded at two different times — second and fifth measurements displayed in lower panel. Lower panel: Object’s visibility (right vertical axis) and equivalent astrophysical null depth (left vertical axis) measured as a function of time. No calibrator star was used; visibilities are derived using the null (or visibility) histogram modeling NSC technique (Hanot *et al.*, 2011; Mennesson *et al.*, 2011a&b, see Sec. 3.1 for details on fitting procedure). All individual visibility error bars are about 0.0006. The final calibrated visibility estimate is  $V = 0.9739 \pm 0.0006$ . The dashed line indicates the astronomical null (or visibility) expected at the same spatial frequency, using  $\alpha$  Boo’s limb darkened diameter measured independently by NIR long baseline interferometry (Perrin *et al.*, 1998; Lacour *et al.*, 2008). A similar method could be applied to CHARA/FLUOR data once the current fringe tracking system (CHAMP) gets connected to FLUOR.

distribution of the instantaneous “null” level (same as interferometric signal described Sec. 3.1, but normalized by constructive interference signal). Interestingly, and as shown in the upper two panels, the observing conditions (beam intensity and phase mismatch) and resulting null level distributions can vary a lot over time, yielding very different average null levels: 0.065 and 0.095 in that case. However, the astronomical null values derived from the NSC fitting method are significantly lower, and much closer to each other:  $0.0130 \pm 0.0005$  and  $0.0132 \pm 0.0006$ . The advantages of the NSC method is that it uses the whole data distribution (not just its average or other ensemble characteristics) to make an estimate of the astronomical null or visibility, and that it takes out the coherence loss effects due to OPD jitter (piston) and intensity mismatch. The final calibrated visibility estimate

derived for  $\alpha$  Boo was  $V = 0.9739 \pm 0.0006$  (astronomical null =  $0.0132 \pm 0.0003$ ), fully consistent with the value expected from its NIR diameter measured at much longer baselines. While such early tests demonstrated the measurements repeatability and overall consistency with previous results (Mennesson *et al.*, 2011b), we also used smaller stars to assess the absolute accuracy of the NSC method. One such case is Vega, whose photosphere is largely unresolved by the PFN 3.2-m baseline, yielding an expected astronomical null of only 0.0004. In comparison, we measured an azimuthally average null of  $0.0008 \pm 0.0004$ , showing that the NSC null measurement error (or any real excess around Vega) is below 0.1% at  $1\sigma$ . The interest of such deep null NSC measurements with the PFN is that no observation of calibrator star is needed to reach an absolute 0.1% accuracy level.

### 3.3. VSC preliminary results at the Keck interferometer

Of course, the PFN is a very favorable system for testing the VSC approach: the telescope AO system acts as a robust fringe tracker, and the interferometric baseline is very short. While a detailed study of the VSC method limitations is beyond the scope of this paper, it is clear that with a  $\gtrsim 10$  times longer interferometric baseline, second order effects will appear, including significant losses of contrast due to finite integration and spectral bandwidth. Unless delay lines are evacuated or a common mount pointing mechanism is used (e.g. LBTI), longitudinal dispersion issues will for instance limit the accuracy of broad-band measurements. In order to have a more realistic idea of the VSC method performance on a long baseline NIR interferometer, we then made some preliminary analysis of KI data, with a projected baseline of 85 m (significantly larger than the nominal 34 m of CHARA/FLUOR). We applied the VSC method to dispersed fringe tracker KI data (5 spectral channels inside the full K-band) obtained on the star HD 175743, a K giant calibrator with a K magnitude of 3.3. These were good quality data with continuous fringe locks of 300 s or more on target. Since the KI fringe tracker uses an “ABCD” modulation scheme (Colavita *et al.*, 1999, 2004) to stabilize phase and group delays, only one of the 4 temporal bins ended up with an OPD position close to the central dark fringe. In addition, during each of the A, B, C or D bin, the OPD was continuously scanned by  $\lambda/4$ , resulting in some constant — easy to calibrate — coherence loss. A full ABCD OPD modulation sequence lasts 4 ms, providing adequate temporal sampling. The photometric and background measurements are typically obtained a minute or so before and after the on-fringe measurements. Although some of these operating conditions were not ideal for applying the VSC method, we found that the derived visibilities were remarkably stable with a standard deviation of 0.18% over 1 hr (10 separate measurements). Figure 3 shows as an example the signal distribution derived for one fringe tracked sequence of 4 min (60,000 points).

### 3.4. Implementing the VSC method at CHARA: CHAMP

In the case of CHARA/FLUOR, most of the VSC working conditions are matched: both beams are eventually recombined into a common single-mode

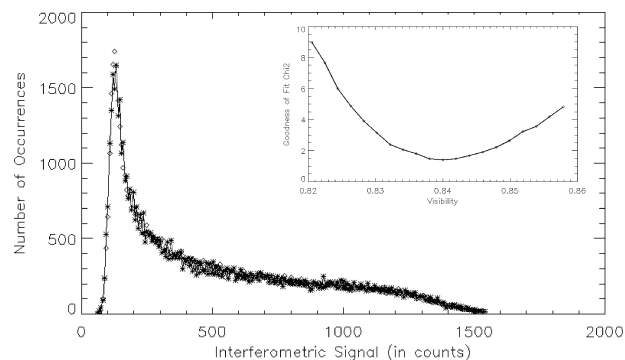


Fig. 3. Distribution of instantaneous interferometric signal values  $I(t)$  recorded on the star HD 175743. Based on Keck Interferometer dispersed fringe tracker data (2.17-micron spectral channel, B bin of ABCD scan). Data points represented by asterisks show the observed number of occurrences in a given signal interval, while diamonds indicate the values obtained for the best fit model distribution derived using the VSC method. The insert shows the residual  $\chi^2$  obtained as a function of visibility, with a best fit value of 0.84 and an uncertainty of  $\sim 0.002$ .

fiber coupler, the resulting interferometric signal is sampled at 500 Hz (much faster than the coherence time of the atmosphere at K-band), the background signal — dominated by a very stable detector dark — is recorded right after the 5 min long fringe acquisition. In addition, the individual beam intensities are measured in real time through FLUOR photometric output channels, which is the ideal case for the statistical analysis. The only ingredient missing is OPD stabilization: FLUOR presently relies on fast scans through the fringe packet and path stabilization within 100 microns, just guaranteeing that each scan contains fringes. Proper application of the VSC will then require to use a fringe tracker in conjunction with FLUOR.

We note that the KI fringe tracking system allowed routine OPD stabilization down to the required level of 200 nm rms or less on an 85-m baseline, and the preliminary results obtained on archival data (Sec. 3.3) make us confident that such performance is also achievable at CHARA. We will likely use the CHARA/MIRC fringe tracker, “CHAMP” (Berger *et al.*, 2008; Monnier *et al.*, 2012), which has already been operated to provide OPD stabilization for MIRC (Monnier *et al.*, 2010), another fiber-based CHARA NIR instrument. For MIRC, the OPD did not need to be stabilized within a fringe, and the FLUOR requirement will be more stringent.

Finally, as in the case of our KI tests, we will start by applying the VSC method to dispersed or

spectrally filtered CHARA/FLUOR data. This will help mitigate dispersion effects, and atmospheric refraction in particular.

#### 4. Example of Faint Excesses Detection and Interpretation

A recurring problem with the interpretation of single baseline interferometric data is the degeneracy between the various models that can fit a given set of observations. In order to further constrain the origin of a possible excess, ancillary observations are required, particularly at different wavelengths and/or spatial resolutions. The simplest interpretation that can be made of high contrast interferometric data is well illustrated in the case of Vega, for which we synthesized the results from 4 different instruments: the Multi-Mirror Telescope (MMT) 10 micron nuller (Liu *et al.*, 2004, 2009), the Keck Interferometer Nuller (KIN, also working around 10 microns), the Palomar Fiber Nuller (PFN, K-band, Mennesson *et al.*, 2011a) and the CHARA/FLUOR instrument. While a circumstellar excess was discovered by CHARA/FLUOR (Absil *et al.*, 2006), no excess was detected by any of the other 3 instruments, and only upper limits were derived. Assuming for instance that the excess detected (or its upper limit) comes from a thin circular dust ring located in the same plane as Vega's

colder disk (seen close to pole-on), one can then compute the ring relative flux (or its upper limit) as a function of distance to the star. As can be seen in Fig. 4 (right), the MMT, KIN and PFN non-detections mean that any ring excess of thermal origin compatible with the detected CHARA excess must reside within 0.15 AU of the star, i.e. very close to the dust sublimation radius around Vega.

By repeating this type of multi-baseline, multi-wavelength studies on a large sample of nearby main sequence stars with NIR excesses detected with CHARA/FLUOR, we hope to further constrain the origin of these excesses and explore the variability of hot exozodiacal disk morphologies, grain composition, temperature and size distributions. This information is a prerequisite to estimate the timescales of the effects affecting the dust grains (collisions, drag forces, sublimation), thus allowing us to constrain the origin of the dust. In this respect, we will make use of all possible synergies between the CHARA/FLUOR and parallel high contrast NIR high resolution imaging programs that some of us are engaged in at CHARA (multiple baseline phase closure imaging with MIRC), at the LBTI (exozodi program follow up observations, shared targets, etc.), and other facilities (high contrast infrared studies with Palomar; exozodi studies with VLTI PIONIER instrument).

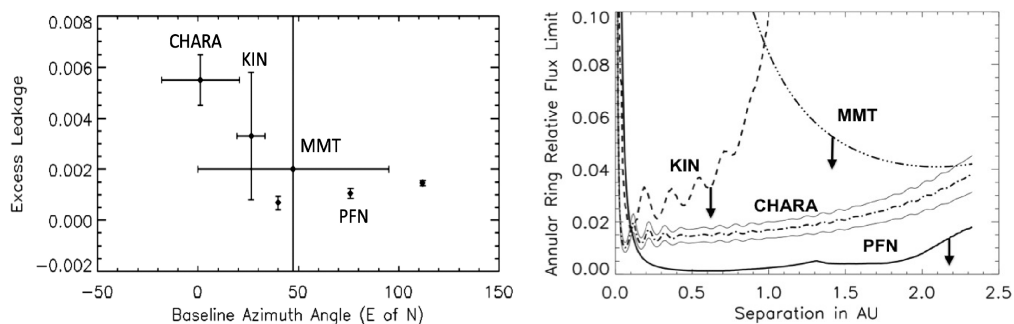


Fig. 4. Left: Excess leakage measured on Vega by various instruments at different baseline orientations (azimuth East of North in degrees). In all cases, the leakage due to the finite size of the star has been subtracted and any “excess leakage” traces possible resolved sources of extra emission. CHARA data use a 34-m baseline at K-band, and show a  $> 5\sigma$  excess. In comparison, no significant excess is detected by the Palomar Fiber Nuller (PFN, 3 lowest points, baseline = 3.2 m, also at K-band), nor by the Keck Interferometer Nuller (KIN, baseline = 85 m,  $\lambda \cong 9 \mu\text{m}$ ) or the MMT (baseline = 4 m,  $\lambda \cong 10.6 \mu\text{m}$ ). Right: Corresponding flux levels (relative to Vega) of a putative geometrically thin dust ring located at various stello-centric distances. The CHARA dash dotted curve (with its bracketing  $\pm 1\sigma$  boundaries) is derived from the excess reported at K-band (Absil *et al.*, 2006). All other curves are ( $3\sigma$ ) upper limits derived from the KIN (9 microns), MMT (10.6 microns) and PFN measurements (the latter using the VSC method discussed in Sec. 3). Assuming no significant changes in the dust distribution between 2005 and 2012, the PFN data constrain the CHARA/FLUOR NIR excess to reside within  $\sim 0.15$  AU of Vega, i.e. very close to the expected dust sublimation radius (similar to Mennesson *et al.*, 2011a, but using the improved June 2012 PFN Vega measurements).

## Acknowledgments

Part of this work was performed at the Jet Propulsion Laboratory, California Institute of Technology, and at the NASA Exoplanet Science Center (NExSci), under contract with NASA. Part of this work is funded through a NASA Origins of Solar Systems grant awarded to B. Mennesson *et al.*, in 2013.

## References

- Absil, O., Mennesson, B., Lebouquin, J. B. *et al.*, 2006, *A&A*, **452**, 237.
- Absil, O. *et al.*, 2008, *A&A*, **487**, 1041.
- Absil, O. *et al.*, 2009, *ApJ*, **704**, 150.
- Absil, O. *et al.*, 2013, *A&A*, **555**, 104.
- Akeson, R. *et al.*, 2009, *ApJ*, **691**, 1896.
- Augereau, J. C. *et al.*, 1999, *A&A*, **348**, 557.
- Backman, D. E. & Paresce, F., 1993, Main-sequence stars with circumstellar solid material — The VEGA phenomenon, In *Protostars and Planets III*, pp. 1253–1304.
- Beichman, C. & Velusamy, T., 1997, *AAS Meeting*, **191**(29), 1310.
- Beichman, C. *et al.*, 2005, *ApJ*, **626**, 1061.
- Berger, D. H. *et al.*, 2008, *Proc. SPIE*, **7013**, 34.
- Beust, H. & Morbidelli, A., 2000, *Icarus*, **143**, 170.
- Colavita *et al.*, 1999, *ApJ*, **510**, 505.
- Colavita *et al.*, 2004, *Proc. SPIE*, **5491**, 454.
- Coude du Foresto, V. *et al.*, 1997, *A&AS*, **121**, 379.
- Coude du Foresto, V. *et al.*, 1998, *Proc. SPIE*, **3350**, 856.
- Defrere, D., Absil, O., Augereau, J. C. *et al.*, 2011, *A&A*, **534**, 5.
- Di Folco, E. *et al.*, 2007, *A&A*, **475**, 243.
- Gomes, R. *et al.*, 2005, *Nature*, **435**, 466.
- Hanot, C., Mennesson, B., Serabyn, E. *et al.*, 2011, *ApJ*, **729**, 110.
- Kelsall, T. *et al.*, 1998, *ApJ*, **508**, 44.
- Lacour, S. *et al.*, 2008, *A&A*, **485**, 561.
- Lebreton, J. *et al.*, 2013, An interferometric study of the Fomalhaut inner debris disk. III. Detailed models of the exozodiacal disk and its origin, Accepted for publication in *A&A*, Astro-ph (arXiv:1306.0956).
- Liu, W. *et al.*, 2004, *ApJ*, **610**, 525.
- Liu, W. *et al.*, 2009, *ApJ*, **693**, 1500.
- McAlister, H. A. *et al.*, 2000, *Proc. SPIE*, **4006**, 465.
- Mennesson, B., Absil, O., Augereau, J. C. *et al.*, 2013, *ApJ*, **763**, 119.
- Mennesson, B. & Mariotti, J. M., 1997, *Icarus*, **128**, 202.
- Mennesson, B. *et al.*, 2002, *JOSA A*, **19**, 596.
- Mennesson, B. *et al.*, 2006, In *Proc. SPIE 6268, Advances in Stellar Interferometry*, eds. Monnier, J. D., Scholler, M. & Danchi, W. C., 95.
- Mennesson, B. *et al.*, 2011a, *ApJ*, **736**, 14.
- Mennesson, B. *et al.*, 2011b, *ApJ*, **743**, 178.
- Merand, A. *et al.*, 2006, *Proc. SPIE*, **6268**, 46.
- Millan-Gabet, R. *et al.*, 2011, *ApJ*, **734**, 67.
- Monnier, J. *et al.*, 2010, *Proc. SPIE*, **7734**, 13.
- Monnier, J. *et al.*, 2012, *Proc. SPIE*, **8445**.
- Nesvorny, D. *et al.*, 2010, *ApJ*, **713**, 816.
- Perrin, G. *et al.*, 1998, *A&A*, **331**, 619.
- Ridgway, S. *et al.*, 2008, *Proc. SPIE*, **7013**, 102.
- Smith, R., Wyatt, M. C. & Haniff, C. A. *et al.*, 2009, *A&A*, **503**, 265.
- Stark, C. C., 2011, *AJ*, **142**, 123.
- Stock, N. D. *et al.*, 2010, *ApJ*, **724**, 1238.
- Thebault, P. & Beust, H., 2001, *A&A*, **376**, 621.
- Wyatt, M. C. *et al.*, 2007, *ApJ*, **658**, 569.